Towards an Estimation of Power Conversion Efficiencies from Surface Sputtering Parameters

Oluwole E. Oyewande
Department of Physics
University of Ibadan
Ibadan, Nigeria.
E-mail: oe.oyewande@ui.edu.ng
Phone: +2349097746152

ABSTRACT

The advent of metal halide perovskites has revolutionised photovoltaic industries owing to their excellent optoelectronic properties and high power conversion efficiency (PCE) of about 25.5%. In this study, Monte Carlo simulation of ion-beam surface sputtering was employed to study sputtering characteristics, such as ion range and sputter yield, of lead and tin perovskites along with other potential materials. This was done to explore the possibility of estimating the PCE of these materials from their surface sputtering characteristics. Since surface sputtering simulations using MC methods are relatively faster and much less computationally expensive than the current standard computational method of determination of PCE using quantum theory and its associated dynamical evolution equations. Results and comparison of the sputtering characteristics for these materials (lead and lead-substituted perovskites inclusive) are presented. For Pb and Sn perovskites, the results revealed similar sputtering characteristics of linear projection ion range with about 78° ion incidence exhibiting maximum sputter yield. The results also showed a correlation between sputter characteristics and PCE.

Keywords: Solar cells; Ion-beam surface sputtering; Perovskites; Sputter yield; Range of ions.

Proceedings Reference Format
Oluwole E. Oyewande (2020): Towards an Estimation of PCEs from Surface Sputtering Parameters. Proceedings of the 27th iSTEAMS Multidisciplinary Innovations & Technology Transfer (MINTT) Conference. Academic City University College, Accra, Ghana. June, 2021. Pp 57-66 www.isteams.net/ghana2021. DOI - https://doi.org/ 10.22624/AIMS/iSTEAMS-2021/V27P7

1. INTRODUCTION

Metal halide perovskites have a wide range of applications in the photovoltaic and optoelectronic industries. In a stable perovskite ABX_3 structure, A-site accommodates a monovalent organic cation (e.g. methylammonium, $CH_3NH_3^+$), B-site accommodates a divalent metallic cation (Pb^+, Sn^+ or Ge^+) while an halide anion (I^-, Br^- or Cl^-) occupies the X-site. Lead halide perovskites has been the focus of intense research for decades. This can be traced to its exceptional optoelectronic properties, high power conversion efficiency (PCE) of about 25.5% [1], cost effectiveness and ease of fabrication [2, 3]. However, the huge gains achieved towards commercialization of metal halide perovskite materials have almost been eroded by the issues of stability and lead (Pb) toxicity. Currently, there is an active search for materials that are not only eco-friendly but also having high resistance against degradations from light, heat and moisture [4 - 9].

Optoelectronic properties of similar material structures have long been investigated to reveal the physical factors responsible for their differences with the popular density functional theory (DFT) approach. However, these properties have not been studied with ion-beam surface sputtering (IBSS) approach even though it is a well-established tool for investigating materials composition and their intrinsic physical differences through secondary ion mass spectroscopy. Thus, an IBSS approach via MC simulation is adopted in this present work. Monte Carlo simulation suites developed by Ziegler and Biersack, Stopping and Range of Ions in Matter (SRIM), and TRansport of Ions in Matter (TRIM), are versatile simulation tools in probing the ion irradiation of materials [10 – 13]. The collision cascade parameters and sputter yield form the signatures of the ion-target interaction. These may change significantly over time with the target composition.

This paper considered six perovskite materials which include $CH_3NH_3PbI_3$ (lead), $CH_3NH_3SnI_3$ (tin), $CH_3NH_3GeI_3$, Cs3Bi2I9, $Rb_3Sb_2I_9$, and $(CH_3(CH_2)_3NH_3)_2CuBr_4$ and studied their ion range and sputter yield for varying ion energies and incident angles. This was done via Monte Carlo simulations implemented in SRIM and TRIM software. Inert gas ions (Ne^+ and Ar^+) were used in the sputtering of the perovskite materials. It is of interest to know the effect of lead replacement on the sputter characteristics of metal halide perovskites. By extension, it is of interest to know whether there is a correspondence between the sputter characteristics and the PCE of the perovskites.

The rest of the paper is structured as follows. Our simulation methods are presented at length in the next section, while our results and discussion are presented section 3. Finally, the conclusion of the study is given in section 4.

2. METHODOLOGY

Details of Monte Carlo simulations as implemented in SRIM and TRIM software are presented in this section. However, the background theory and simulation algorithms forming the working principle behind SRIM and TRIM software are well discussed in the package supporting papers by Ziegler and Biersack [10 - 13]. For the inert gas ions (Ne^+ and Ar^+), the ion range were simulated using SRIM at normal incidence angle with the variation of ion energies from 1 keV to 10 keV on the target. Typical ion energies in the range of 1 keV to 10 keV are the ones used for sputtering experiments as ion energies below this range (eg 500 eV) are classify under low-energy sputtering experiment. Here, lead and tin perovskites ($CH_3NH_3PbI_3$ and $CH_3NH_3SnI_3$) were used as targets. The bombardment of the target perovskites by the incident ions yielded different components each of which were simulated by means of TRIM for varying incident angles from 0^o to 100^o and incident ion energies of 1 keV and 5 keV

The thickness of perovskite wafer used in TRIM set-up was 35 nm. The composition of the perovskite targets (lead, tin and germanium) were used to build the target wafer using stoichiometric ratio of 1:3:1:3:1:3 for C, H, N, H, Pb/Sn/Ge and I respectively for both SRIM and TRIM simulations. For lead and tin perovskites, experimental values of their densities from literature were used as 4.16 g/cm^3 and 3.51 g/cm^3 [14 - 15] respectively. For germanium and other perovskites, TRIM was used for calculation of their densities due to unavailability of experimental values from literature. The reality of densities calculated via TRIM was validated by calculating the densities of lead and tin perovskites (2.49 g/cm^3 and 2.15 g/cm^3) which revealed underestimation of about 40 % to experimental values.

Therefore, a correction factor of 5/3 was used to convert the calculated values with the density of germanium perovskite now 3.32 g/cm^3 instead of 1.99 g/cm^3 which was calculated originally.

A ratio of 2:6:6:12:2:6:1:4 was used to build $(CH_3(CH_2)_3NH_3)_2CuBr_4$ perovskite from its composition for C, H, C, H, N, H, Cu and Br in TRIM and SRIM using the density of 1.87 g/cm^3 corrected from the calculated value of 1.12 g/cm^3 using the same correction factor. For the composition of $Rb_3Sb_2I_9$ and $Cs_3Bi_2I_9$ perovskites, 3:2:9 stoichiometric ratio was used for Rb/Cs, Sb/Bi and I, respectively. Their corrected densities from the calculated values of 4.46g/cm^3 and 4.98g/cm^3 were 7.43g/cm^3 and 8.30g/cm^3 respectively. To allow for a reasonable simulation run time, 1000 ions were used for each simulation. Calculation of sputter-yield was done in TRIM set-up by performing "Monolayer Collision Step/Surface Sputtering" while calculation of the projected range was done by performing full cascade damage calculation in the SRIM set-up.

3. RESULTS AND DISCUSSION

Discussion of results obtained from our simulation studies is presented in this section. Ne^+ and Ar^+ ions were used for sputtering and the results revealed a similar trend for both ions, with Ar^+ion showing lower values of ion range but higher values of sputter yield than Ne^+ ion. In Figures 1-7, the results of Pb perovskite are presented along with those of Sn perovskite being the most promising substitute for Pb. The rest of the results for other perovskites with lower PCEs are present in Figure 8-11. The linear ions projected range in Pb and Sn perovskites were observed to be very close in values across the varying incident energies from 1 keV to 10 keV. This similarity in linear ion range values was very obvious with Ar^+ ion sputtering (see Figure 1). It is an indication that Sn could be a good substitute for Pb in $CH_3NH_3PbI_3$ perovskite. The similarity in linear ion range values for the two perovskites could be that they possess similar stopping power to energetic particle bombardment.

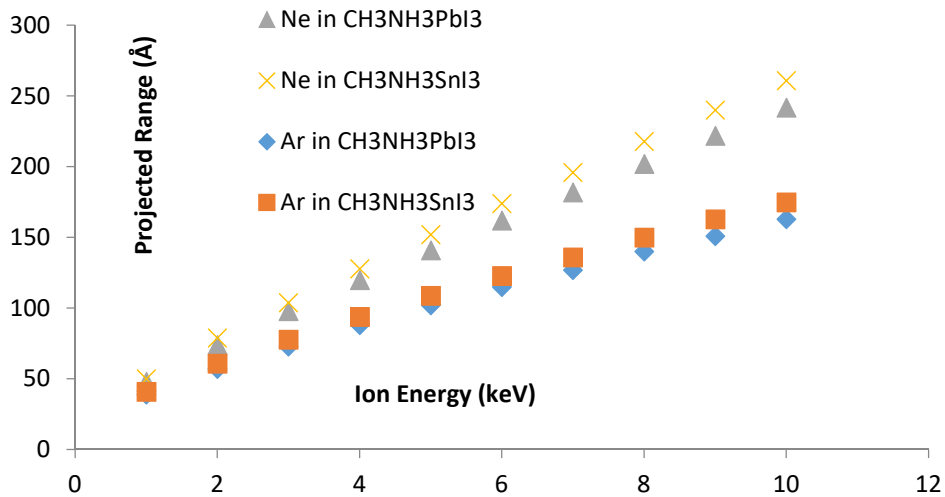

Figure 1: Ne$^+$ and Ar$^+$ ion projected range for varying incident ion energies from 1 keV to 10 keV in lead- and tin-perovskite targets.

In the following Figures (2 – 7), the simulated results of sputter yield for each elemental components in the perovskite are presented (one for each of the elements). These elements include C, H^1 for the methyl molecule, N, H^2 for the ammonium molecule, Pb/Sn, and I. The results presented here is for the number of ejected atoms per Ne^+ and Ar^+ ions with incidence ion energies of 1 keV and 5keV applied on Pb and Sn perovskites at various incidence angles from 0° to 89°. The results revealed higher sputter yield for the higher incident ion energy of 5 keV for all the elements involved (see Figures 2 – 7). It is also observed that sputter yield increased steadily as the incidence angle was increased and reached a maximum around 78° incidence angle with a little declination after this value. The summary of the range of sputter yield (atom/ion) across the various angles of incidence for each element at 1 keV and 5keV incidence ion energies is presented in Table 1.

Table 1: The range of sputter yield (atom/ion) across the various angles of incidence (°) for each element at 1 keV and 5keV incidence ion energies.

	C	H^1	N	H^2	Pb/Sn	I
1 keV	0.03 – 0.20	0.24 – 0.86	0.16 – 0.46	0.24 – 0.89	0.13 – 0.53	0.45 – 1.76
5 keV	0.08 – 0.43	0.50 – 1.95	0.21 – 1.21	0.50 – 2.10	0.21 – 1.21	1.05 – 4.09

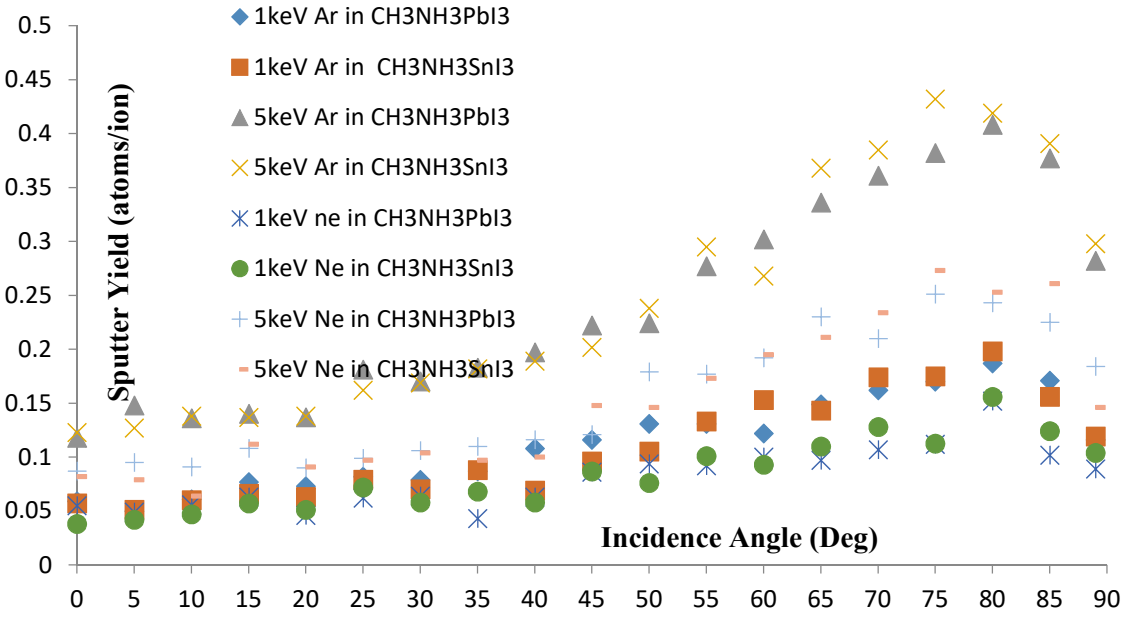

Figure 2: Sputter yield of C atoms (for the ejection of C atoms) per Ar^+ and Ne^+ irradiation of the perovskites at 1 keV and 5 keV for different incident angles.

The maximum sputter yield (atoms/ion) of the elements for both incident ion energies (1keV and 5keV) as is observed from Figures 2 – 7 is in the order C < N < Pb/Sn < H^1 < H^2 < I. This order of maximum sputter yield can easily be confirmed from values listed in Table 1.

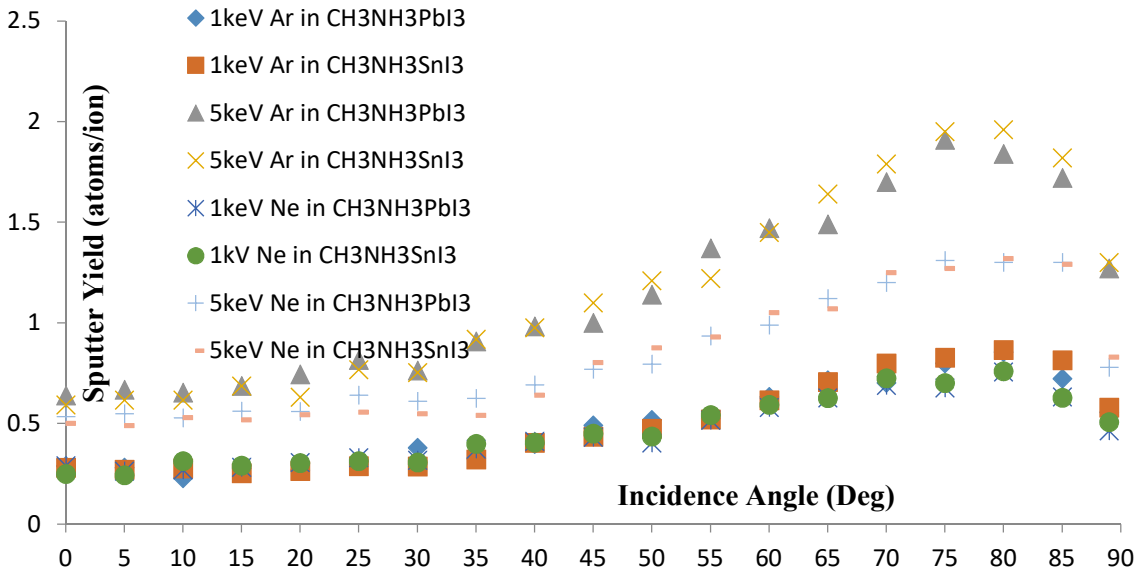

Figure 3: Sputter yield of H^1 atoms (for the sputter erosion of H atoms of the methyl molecule) per Ar^+ and Ne^+ irradiation of the perovskites at 1 keV and 5 keV for different incident angles.

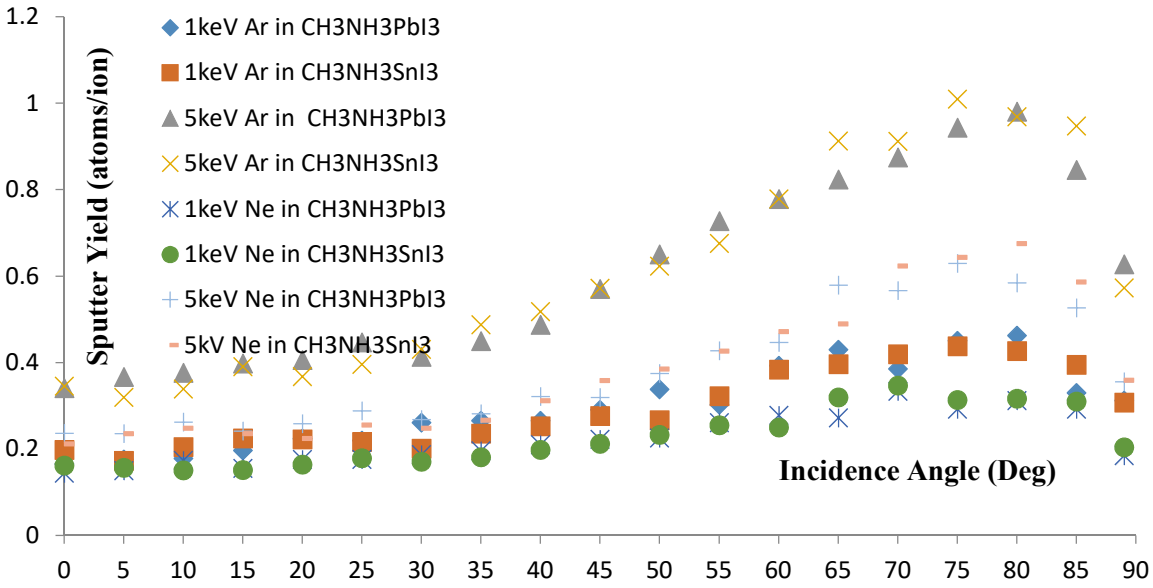

Figure 4: Sputter yield of N atoms (for the erosion of N atoms) per Ar^+ and Ne^+ irradiation of the perovskites at 1 keV and 5 keV for different incident angles.

The hydrogen atoms of the methyl and ammonium molecules have relatively similar values of sputter yield with that of methyl molecule (i.e. H^1) having a slightly lower value.

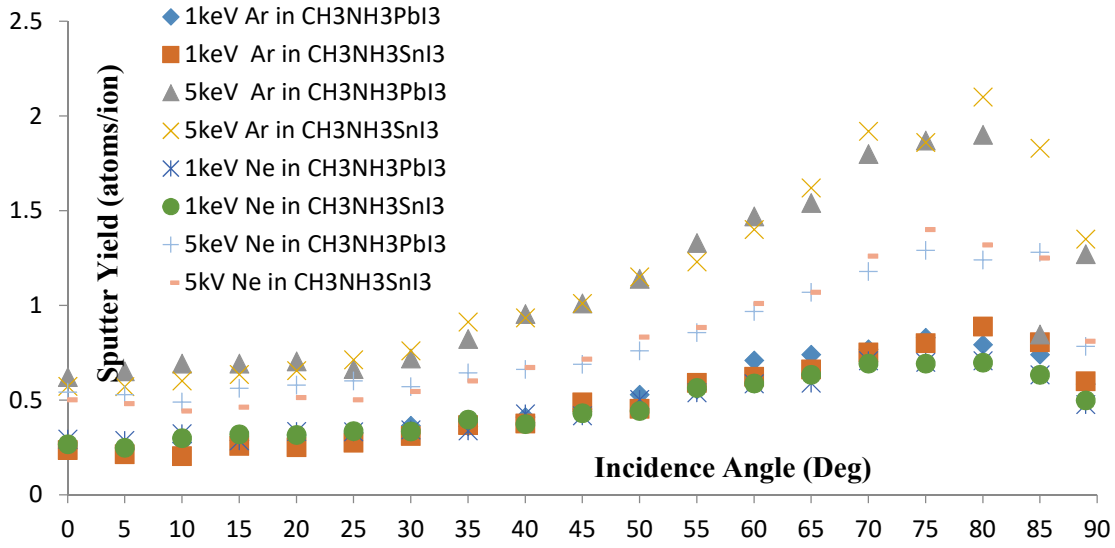

Figure 5: Sputter yield of H^2 atoms (for the ejection of H atoms of the ammonium molecule) per Ar^+ and Ne^+ irradiation of the perovskites at 1 keV and 5 keV for different incident angles.

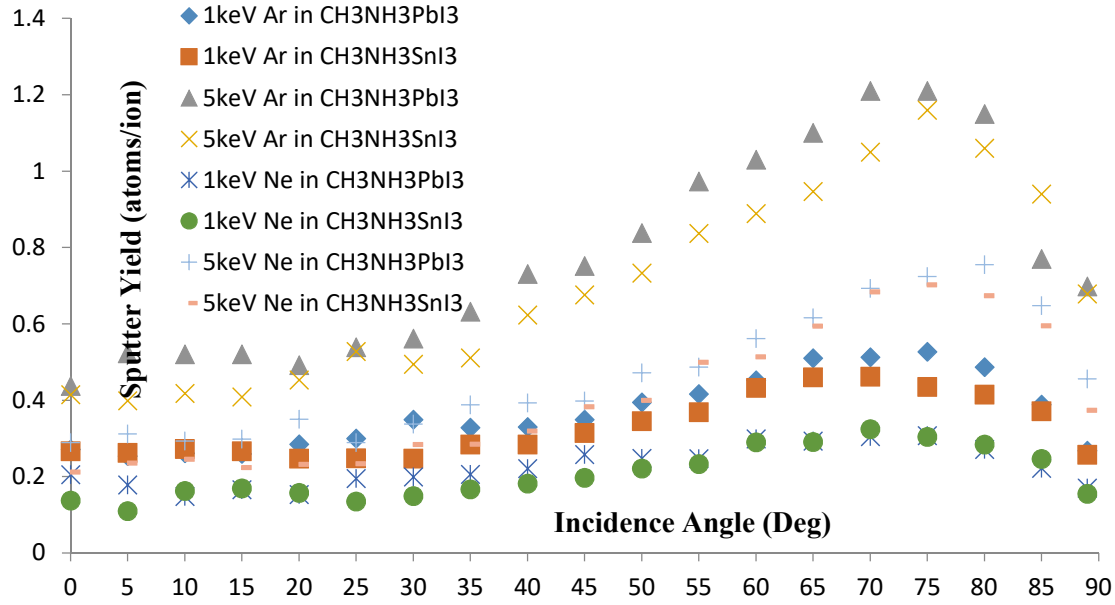

Figure 6: Sputter yield of Pb/Sn atoms (for the erosion of Pb/Sn atoms) per Ar^+ and Ne^+ irradiation of the perovskites at 1 keV and 5 keV for different incident angles.

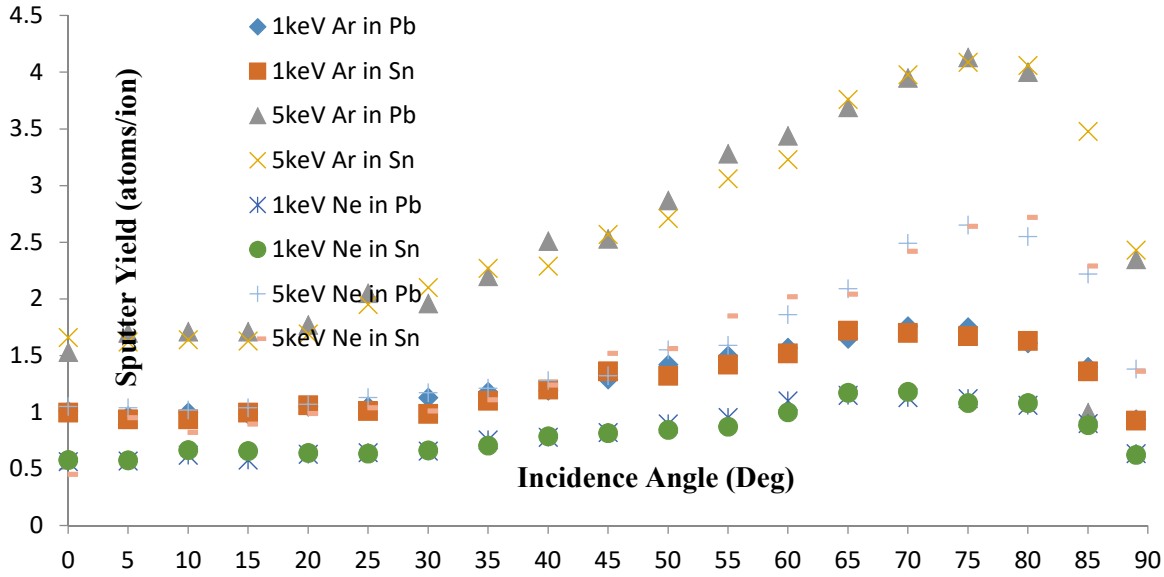

Figure 7: Sputter yield of I atoms (for the erosion of I atoms) per Ar^+ and Ne^+ irradiation of the perovskites at 1 keV and 5 keV for different incident angles.

In the following Figures 8 – 11, the sputtering results of the perovskites with lower PCEs which include $CH_3NH_3GeI_3$, Cs3Bi2I9, $Rb_3Sb_2I_9$, and $(CH_3(CH_2)_3NH_3)_2CuBr_4$ are presented. The results showed a similar trend of values for both Ne^+ and Ar^+ ion sputtering over the entire range of incident angles as well as the incident ion energies of 1 keV and 5 keV. Therefore, the sputtering results presented and discussed here are only those for Ne^+ and 1 keV incident ion energy.

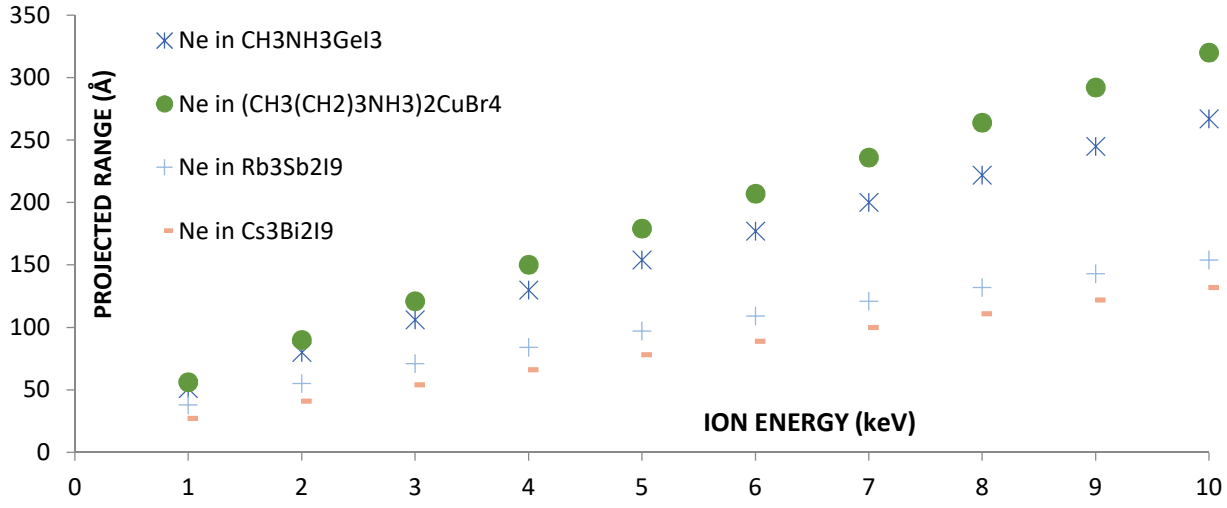

Figure 7: Ne^+ projected range for the remaining perovskites at different ion energies (1 keV - 10 keV).

The results presented in Figure 8 are for the projected ion range in the above mentioned perovskites. The increase in the projected ion range of these perovskites followed the trend of their increasing PCEs which are reported in Ref [3]. However, a slight deviation from this trend is observed from the curve of $(CH_3(CH_2)_3NH_3)_2CuBr_4$ perovskite having a reported PCE of 0.63%. As such, it is expected to fall between the curves of $Rb_3Sb_2I_9$ and $CH_3NH_3GeI_3$ perovskites having reported PCEs of 0.66% and 0.20% respectively. It can therefore be inferred from this result that the projected ion range values correlate only with the PCE values of the perovskite with the same halide occupying the X-site.

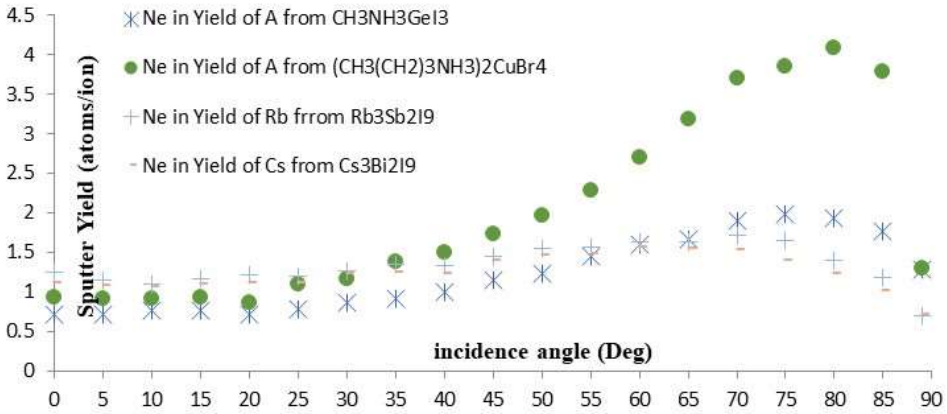

Figure 9: Sputter yield of A cations (for the erosion of A cations) per Ar^+ and Ne^+ irradiation of the remaining perovskites at 1 keV and 5 keV for different incident angles.

In Figures 9 – 11, sputter results of these perovskites as functions of incident angles are presented for Ne^+ ion sputtering at 1 keV incident ion energy as mentioned before. Owing to the fact that Cu and Sb are heterogeneous cations and their host perovskites are compose of different halide at the **X**-site, results of sputter yield for the different elements are not presented in details as done for Pb and Sn perovskites. Instead, results of sputter yield are presented base on occupational site of the constituent elements. That is, results for the sputter yield for **A**-site, **B**-site, and **X**-site are presented in Figures 9, 10 and 11 respectively.

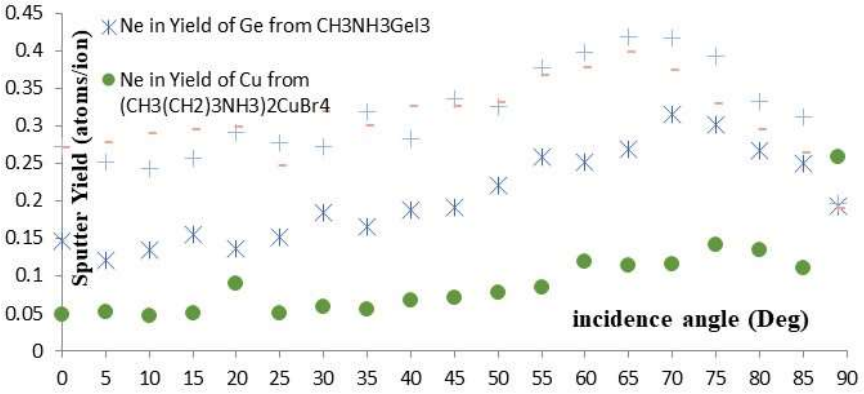

Figure 10: Sputter yield of B cations (for the erosion of B cations) per Ar^+ and Ne^+ irradiation of the remaining perovskites at 1 keV and 5 keV for different incident angles.

Beyond the critical angle of $\sim 78°$ for maximum yield, similar trends are observed for the sputter yields for **A** and **B** cations (as depicted in Figures 9 and 10 respectively), supporting our earlier deduction of correspondence between sputtering characteristics and PCEs. In Figures 9 -11, the yield tends to decrease with increasing efficiency, with the exception to the Cu-based perovskite. However, the yield for Bi and Sb perovskites seems to be less vague as seen in Figure 11. Thus, the results of this study indicate a correspondence (direct or inverse) between the sputter characteristics and PCE.

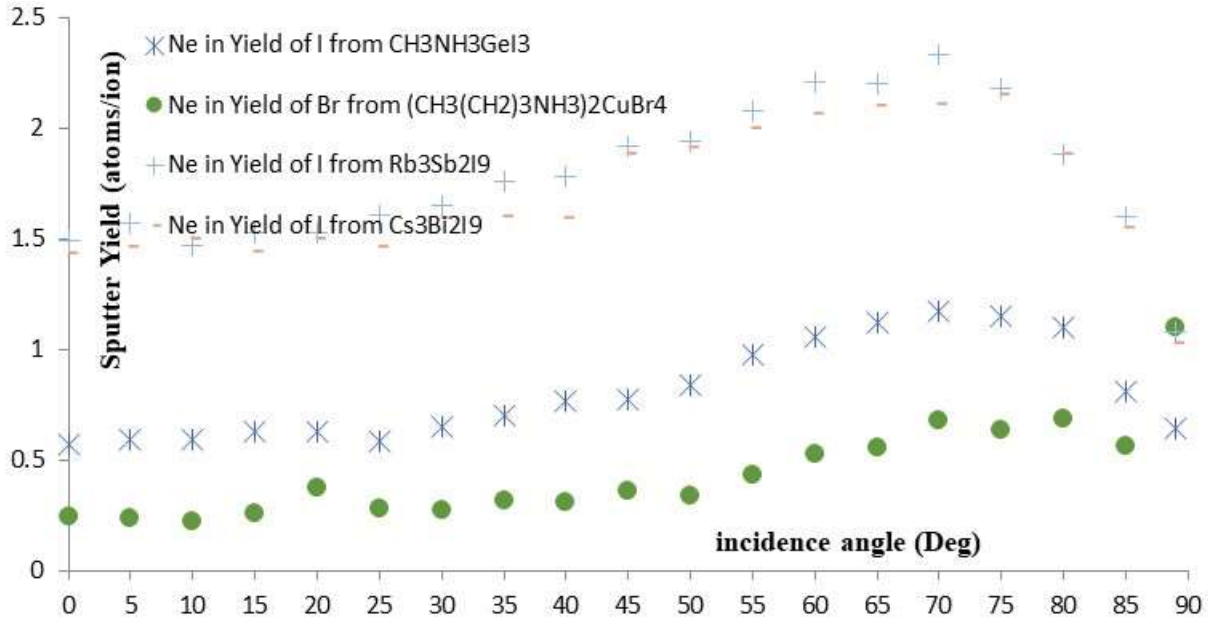

Figure 11: Sputter yield of X anions (for the erosion of X anions) per Ar^+ and Ne^+ irradiation of the remaining perovskites at 1 keV and 5 keV for different incident angles.

4. CONCLUSION

Ion sputtering simulation of $CH_3NH_3PbI_3$, $CH_3NH_3SnI_3$ $CH_3NH_3GeI_3$, Cs3Bi2I9, $Rb_3Sb_2I_9$, and $(CH_3(CH_2)_3NH_3)_2CuBr_4$ perovskites has been performed based on Monte Carlo algorithm implemented in SRIM and TRIM software package. This is done as a new approach towards assessing the interesting physical properties of lead-based perovskite as well as the possibility of substituting lead with less toxic elements. The less toxic element substitutes for lead currently exhibit much lower PCEs as compare to their lead counterpart. However, its Sn substitute exhibits very similar sputter yield characteristics corresponding to their PCEs putting it as the best substitute for lead as found in this study, though a lower PCE of 6.4% was reported for it [5]. This corroborates the most reason why tin perovskite should be looked into with the aim of improving its properties towards enhancing its PCE for a better solar cell application even though it has low PCE currently. The results thus confirmed sputter yield characteristics correspondence with the PCEs of the perovskites.

REFERENCES

[1] National Renewable Energy Laboratory (NREL), Best Research-Cell Efficiency Chart (2021), https://www.nrel.gov/pv/cell-efficiency.html. (Rev. 01-04-2021)
[2] S. Casaluci, L. Cinà, A. Pockett, P. S. Kubiak, R. G. Niemann, A. Reale, A. Di Carlo, and P. Cameron, J. Power Sources **297**, 504 (2015).
[3] S. Hoefler, G. Trimmel, and T. Rath, "Progress on lead-free metal halide perovskites for photovoltaic applications: a review," *Monatsh Chem.,* vol. 148, pp. 795, 2017.
[4] H. J. Snaith,, *J. Phys. Chem. Lett.*, vol. 4, no. 21, pp. 3623–3630, 2013.
[5] N. Noel, S. Stranks, A. Abate, C. Wehrenfennig, S. Guamera, A. Haghighirad, A. Sadhanala, G. Eperon, S. Pathak, M. Johnston, A. Pertozza, L. Herz, and H. Snaith, *Energy Environ. Sci.,* vol. 7, pp. 3061, 2014.
[6] T. Krishnamoorthy, H. Ding, C. Yan, W. Leong, T. Baikie, Z. Zhang, M. Sherburne, S. Li, M. N. Asta, and S. Mhaisalkar, *J Mater Chem.,* vol. A3, pp. 23829, 2015.
[7] X. Cui, K. Jiang, J. Huang, Q. Zhang, M. Su, L. Yang, Y.-L. Song, X.-Q. Zhou, and M. Synth*,* vol. 209, pp. 247, 2015.
[8] B. Park, B. Philippe, X. Zhang, H. Rensmo, G. Boschloo, and E. Johansson, *Adv. Mater,* vol. 27, pp. 6806, 2015.
[9] P. Harikesh, H. Mulmudi, B. Ghosh, T. Goh, Y. Teng, K. Thirumal, M. Lockrey, K. Weber, T. Koh, S. Li, S. Mhaisalkar, and N. Mathews, *Chem. Mater,* vol. 28, pp. 7496, 2016.
[10] J. Ziegler, and J. Biersack, "TRIM," *SRIM*.
[11] J. Ziegler, M. Ziegler, and J. Biersack, "The stopping and range of ions in matter," *Nucl. Instrum. Meth. Phys. Res. B,* vol. 268, pp. 1818-1823, 2010.
[12] S. Martinie, T. Saad-Saoud, S. Moindjie, D. Munteanu, and J. Autran, "Behavioral modeling of SRIM tables for numerical simulation," *Nucl. Instrum. Meth. Phys. Res. B,* vol. 322, pp. 2-6, 2014.
[13] W. Wilson, L. Haggmark, and J. Biersack, "Calculations of nuclear stopping, ranges, and straggling in the low-energy region," *Phys. Rev. B,* vol. 15, pp. 2458, 1997.
[14] J. Huang, K. Jiang, X. Cui, Q. Zhang, M. Gao, M. Su, and L. Yang, "Direct conversion of of CH3NH3PbI3 from electrodeposited PbO for highly efficient planar perovskite solar cells," *Sci. Rep.,* vol. 5, pp. 15889, 2015.
[15] C. Kim, T. Huan, S. Krishnan, and A. Ramprasad, "A hybrid organic inorganic perovskite dataset," *Sci. Data* vol. 4, pp. 170057, 2017.